OPTICAL FILTER DESIGN: GAIN ANALYSIS AND TOLERANCE ANALYSIS

A Thesis

by

VIVEK VANDRASI

Submitted to the Office of Graduate Studies of
Texas A&M University
in partial fulfillment of the requirements for the degree of

MASTER OF SCIENCE

August 2010

Major Subject: Electrical Engineering

OPTICAL FILTER DESIGN: GAIN ANALYSIS AND TOLERANCE ANALYSIS

A Thesis

by

VIVEK VANDRASI

Submitted to the Office of Graduate Studies of
Texas A&M University
in partial fulfillment of the requirements for the degree of

MASTER OF SCIENCE

Approved by:

Co-Chairs of Committee,	Christi K. Madsen
	Ohannes Eknoyan
Committee Members,	Scott Miller
	Alexey Belyanin
Head of Department,	Costas Georghiades

August 2010

Major Subject: Electrical Engineering

ABSTRACT

Optical Filter Design: Gain Analysis and Tolerance Analysis. (August 2010)

Vivek Vandrasi, B.Tech, Indian Institute of Technology Guwahati

Chair of Advisory Committee: Dr. Christi K. Madsen

Three components, gain analysis, tolerance analysis in-depth, and a brief non-linearity analysis, are presented. In the first component, the effects of an Erbium doped waveguide amplifier in a microring are investigated using a time domain simulation. Methods to simulate the gain versus average input signal power in the microring are studied, given that it has a long lifetime compared to the short delay time of the microring. The methods are based on the dependence of the gain on the power of the signal being fed to the ring.

An algorithm is proposed to perform a thorough tolerance analysis on any optical circuit with respect to any optical parameter. The algorithm, based on Monte Carlo Simulation, is implemented on a complex optical circuit that is designed to obtain a bandpass filter response of given specifications. It is also tested on similar designs for a comparative study between them. The parameters and the structure of the designs used for the analysis are presented in detail. The results are presented in terms of the yield with respect to the parameter being varied, against their tolerance value.

Algorithms for studying the effects of two types of non-linearities are presented. The Kerr nonlinearity and the two-photon absorption are included in the bandpass filter designs used for the tolerance analysis. The algorithms are based on the power circulating in different regions of the circuit under consideration. The variation in the original response because of the loss due to nonlinearity is observed and analyzed for different power levels of the input signal.

ACKNOWLEDGMENTS

Foremost, I would like to express deep gratitude to my advisor Dr. Christi K. Madsen for introducing me to the field of photonics and supporting me throughout the M.S. study. I would also like to thank Dr. Ohannes Eknoyan, Dr. Scott Miller and Dr. Alexey Belyanin for accepting to be my committee members.

Besides the professors, my sincere thanks to the post docs, Shun Hui and Rohit Patnaik, and fellow graduate student, Ivan Zhou, for their guidance and stimulating discussions. I would like to mention my roommates, Bharath, Sandeep, and Sireesh, for all the fun we had through the two years, and for keeping me alive and excited.

Last but not the least, I will always be grateful and appreciative to my parents and my sister, who have been there for me all my life.

TABLE OF CONTENTS

CHAPTER Page

LIST OF TABLES

LIST OF FIGURES

FIGURE Page

CHAPTER I

INTRODUCTION

This thesis establishes procedures to study the introduction of gain into a microring and to implement tolerance and nonlinearity analyses on different optical filter designs. In order to do so, the optical designs are first modeled in terms of digital filters, as explained in Chapter II. It also presents a survey on the literature on this topic along with a few examples. This modeling helps in analyzing complex optical circuits easily in terms of poles and zeros.

Erbium doped fiber amplifiers and Erbium doped waveguide amplifiers are being widely used in order to compensate for losses in various optical devices. A review of the literature on EDWA is presented in Chapter III. The life time of the Erbium ion excitation is on the order of milliseconds as opposed to the small delay time of a microring on the order of nanoseconds. Hence, it would require on the order of 10^7 delays in order to make sure that the gain is activated in the ring to the average power. The dependence of the gain on the input signal power to the ring's feedback path plays an important role in this matter. Instantaneous power and average signal power are both considered in a time domain analysis of the structure.

Robustness of a design is primarily studied at large in mechanical and industrial engineering fields. A design can be said to be robust if the effect of any type of variations in the components of the design on the final output is minimal. The importance of this factor in an optical design has been emphasized at times in the past. The limit to the precision in the fabrication of an optical circuit, in terms of the parameter values, is the reason for the tolerance study that is presented in Chapter

---

The journal model is *IEEE Transactions on Automatic Control.*

IV. The effect of variation in a parameter on the final response can be theoretically understood by studying its effect on the location of poles and zeros, from a high level perspective.

The effect of nonlinearities on the optical designs is studied to a limited extent. Only two types of nonlinearities, Kerr nonlinearity and two photon absorption effects are studied. The loss incurred due to them add up to the inherent losses of the design and cause the distortion in the final response from what is expected.

CHAPTER II

OPTICAL FILTERS AS DIGITAL FILTERS

The optical filter design can be effectively modeled in terms of digital filter design. The methods used to analyze digital filters can be used for optical filters by simple transformations. Some of the commonly used transformations are modeling as a z-transform, a transfer matrix and a graphical representation. Section A gives an overview of the literature on these methods and presents the representation of the transfer functions of simple optical structures as z-transforms. A transfer function is the output response with respect to the input signal. This chapter presents and uses the discrete time system properties of digital filters.

A. Literature Review

Use of z-transforms to model optical circuits is first discussed in [1]. It presents an overview of the z-transform properties and justifies its usage to model optical circuits. The transfer functions for a two-coupler recirculating delay line with all four combinations of output over input are represented using the transform and gives a pole-zero analysis of the same.

A transfer-matrix method has been proposed in [2] to model optical circuits. The concept of equating the fields at a point has been modified to reduce the computational complexity of the algorithm. An analysis of the fiber ring resonators using this algorithm has been presented. A state space algorithm is used in [3] and tested on a narrowband filter transfer function. A graphical representation method is proposed in [4]. This algorithm proves to be a quicker way to represent the transfer functions and analysis of resonance effects.

The z-transform modeling has been used in [5] to obtain transfer functions for

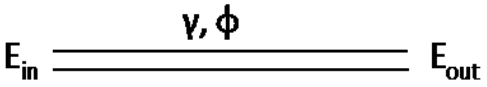

Fig. 1.: Waveguide

a microring and Fabry Perot interferometer. The lossless all-pass filters are analyzed and are used as building blocks for the design of multistage structures with higher number of poles and zeros. Additional uses of digital signal processing techniques in optical filter design are documented in [6]. The work in section B is explained in detail in [7].

B. Z-transform

A waveguide is always associated with a loss term(γ) and a phase term(ϕ). The phase change results upon the signal passing through the waveguide. For the straight waveguide shown in Fig. 1, the transfer function can be represented as

$$H = \frac{E_{out}}{E_{in}} = \gamma e^{-j\phi} \tag{2.1}$$

where E_{out} and E_{in} represent output and input electric field of a singlemode waveguide. The phase term of this optical structure can be written as z^{-1}, making the transfer function,

$$H = \frac{E_{out}}{E_{in}} = \gamma z^{-1} \tag{2.2}$$

For any optical circuit, each waveguide transfer function can now be written as a z-transform. Fig. 2 shows a microring structure, where a straight waveguide is coupled to a circular waveguide at a single point. Upon using simple algebra, its

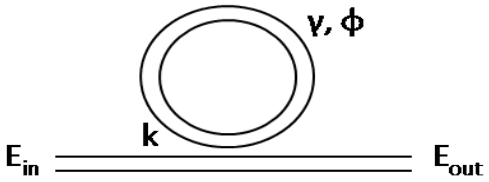

Fig. 2.: Strucutre of microring

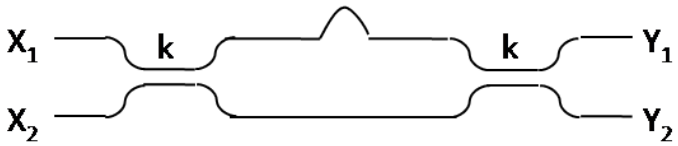

Fig. 3.: Mach-Zehnder interferometer

transfer function shows that the structure is a single pole-single zero filter.

$$H = \frac{E_{out}}{E_{in}} = \frac{c - \gamma z^{-1}}{1 - c\gamma z^{-1}}, c = \sqrt{1-k} \tag{2.3}$$

where c represents the bar-state transmission of the coupler and k represents the cross-state power transfer.

The approach has been used for an asymmetric Mach-Zehnder Interferometer, shown in Fig. 3, which is similar to a two-port network. Each of the four transfer functions possible are written in matrix form as

$$\begin{pmatrix} Y_1 \\ Y_2 \end{pmatrix} = \begin{pmatrix} -s^2 + c^2 z^{-1} & -jcs(1+z^{-1}) \\ -jcs(1+z^{-1}) & c^2 - s^2 z^{-1} \end{pmatrix} \begin{pmatrix} X_1 \\ X_2 \end{pmatrix} \tag{2.4}$$

These are similar to FIR digital filters with a single zero and and a pole at zero. The transfer functions are obtained for identical couplers in the MZI. It can be observed in this case that H_{12} and H_{21} always have a zero on the unit circle.

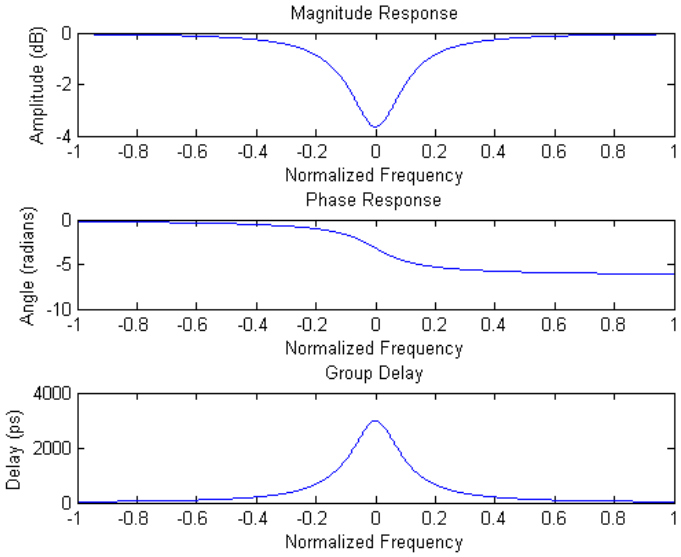

Fig. 4.: Response of microring structure (normalized units versus physical units: time is scaled by T and frequency by FSR)

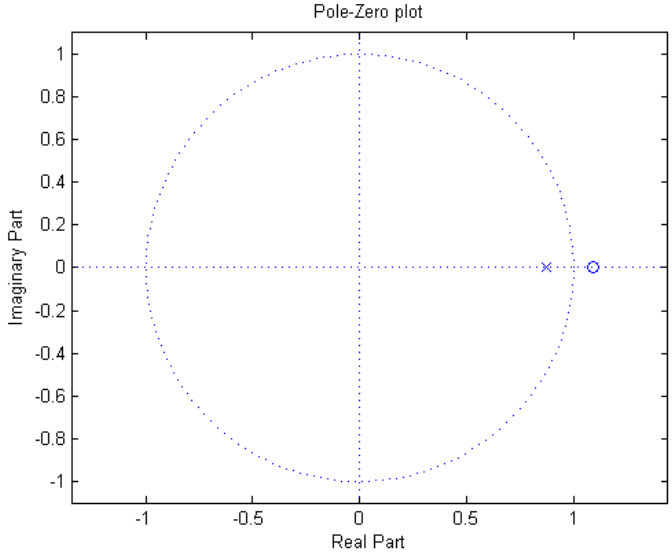

Fig. 5.: Pole-zero plot for microring structure

Fig. 4 shows the magnitude, phase responses and the group delay for a microring structure using z-transform analysis. The coupling value used is $k = 0.2$, whereas the loss is set to $\gamma = 0.9772$. The pole-zero plot is shown in Fig. 5. The pole is located at γc, inside the unit circle, and the zero at γ/c.

Any extra phase terms in an optical circuit resulting because of a phase shifter can be added to the original phase term, represented by z^{-1}, as $e^{-j\phi}z^{-1}$.

CHAPTER III

GAIN ANALYSIS

EDWA, the Erbium doped waveguide amplifier, is an important means to amplify a signal in optic communication systems. The transmission over long distances of Wavelength Division Multiplexed (WDM) channels, which increases the capacity of optic systems, is made possible by Er-doped fiber amplifiers. Optical amplifiers are a great addition to integrated optics. They serve as integration to other devices like waveguides, couplers and multiplexers. The losses in such passive devices may be compensated with the gain from these optical amplifiers.

A. Literature Review

Erbium doped fiber amplifiers and Erbium doped waveguide amplifiers are being extensively studied. EDFA is used for optical fiber communications and is suited for many circumstances. EDWA and other amplifiers are used for specific environments. Although not directly the same, EDWA uses a similar concept as EDFA. EDWA has advantages over EDFA in terms of lower cost and size. It brings a higher gain through a shorter waveguide unlike in EDFA which requires several meters of fiber.

There are several parameters that effect the gain from the EDWA. This has been discussed in [8]. The Erbium concentration and solubility, the loss in the waveguide, mode overlaps and the pump wavelength are the important ones. The solubility of Er has to be high in the substrate in order to achieve high gain. One of the materials that are suited for this process is silica glass. The waveguide loss is an equally important factor. This loss needs to be compensated before a gain can be achieved in the device. The wavelength at which the Erbium ions are pumped to excited states effects the strength of the stimulated emission.

Planar waveguide amplifiers with different materials doped into different substrates have been illustrated in [9]. The working and the performances of those amplifiers at various parameter values have been presented. In a more recent paper [10], a review of various optical amplifiers has been done. Erbium doped fiber amplifiers (EDFA), Fiber Raman amplifiers (FRAs), Erbium doped waveguide amplifiers (EDWAs) and semiconductor optical amplifiers (SOAs) are among the ones that have been discussed and compared with an overview of the parameters that influence their properties like gain and their applications.

The fabrication of an EDWA using the concepts of EDFA has been discussed in [11]. Only a few numerical algorithms have been available at the time for the computation of amplification in EDWA. It gives a brief introduction to the physics behind the planar waveguides and moves on to develop a model for implementing an EDWA. The model has been tested for a special case of EDFA. Quite a lot of research has been done on developing methods to fabricate planar waveguides and a number of papers have been published on the same. Apart from the fabrication, the gain models for EDWA have been discussed in a few papers. [12] presents the distribution of gain in silica based planar waveguide. Optical small signal net gain has been dealt with in [13].

The research done has mainly focussed on a fabrication point of view. This project deals with the effects of Erbium doping in a microring resonator using a simulation-level analysis.

B. Passive Case

The structure of the microring with gain is shown in Fig. 6. The input energy of the signal is represented by E_{in} and the output of the structure is represented by

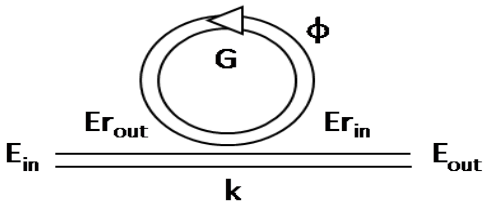

Fig. 6.: Lossless microring with gain

E_{out}. Similarly, the input electric field entering the ring is denoted by Er_{in} and the energy leaving the ring by Er_{out}. In the passive structure, the gain is set to zero. The transfer function in this case can be obtained through its visualization as a 2-port network with a feedback path. It is given, for a lossless ring, by Equation 3.1.

$$H = \frac{Eout}{Ein} = \frac{c - z^{-1}}{1 - cz^{-1}}, c = \sqrt{1-k}, s = \sqrt{k} \tag{3.1}$$

where k stands for the amount of coupling into the ring and z^{-1} denotes the phase change due to traversing the ring.

On the other hand, it can also be obtained by using an iterative procedure in the time domain, by adding the output generated after each loop around the ring. This can be written in the form of Equation 3.3.

$$E_{out} = (c\delta(n) + (-js)(-js)\delta(n-1) + (-js)c(-js)\delta(n-2) + ...)E_{in} \tag{3.2}$$

Applying z-transform on Equation 3.2 gives rise to a summation in frequency domain, as shown in Equation 3.3.

$$H = c + (-js)z^{-1}(-js) + (-js)z^{-1}cz^{-1}(-js) + ... = \frac{c - z^{-1}}{1 - cz^{-1}} \tag{3.3}$$

For a lossy structure, the term z^{-1} is replaced by γz^{-1} where γ represents the loss in the ring waveguide.

C. Amplifier

A gain is introduced into the ring through the excitation of erbium ions by a pump laser. The gain is activated when the input signal transmission results in a stimulated emission of the erbium ions. The amount of gain has been found to be dependent on the power of the input signal. During the time for the ring to reach a steady state, the signal power circulating in the ring changes the amount of gain and lets it saturate as the ring itself reaches the steady state. For an input signal E_{in}, this dependence has been approximated as an exponential model, shown in Equation 3.4.

$$G = e^{\frac{G_0 L}{1+\frac{\Sigma Pr_{out}/N}{P_{in}}}} \tag{3.4}$$

where G_0 is a constant, $\Sigma Pr_{out}/N$ is the average power that has circulated in the ring until that iteration of the loop, P_{sat} is the saturation power and L is the perimeter of the ring. The value of G_0 is chosen so that the net loss in the ring denoted by γ is always strictly less than 0.98.

The value of effective loss, γ, varies with the amount of gain during that iteration. As the signal traverses the ring, at any iteration 'm' of the loop, the amount of power entering the ring, $Pr_{in}(m)$, is measured in terms of the amount of power entering the ring in the previous iteration, $Pr_{in}(m-1)$ as in Equation 3.10. By calculating the power leaving the ring, Pr_{out}, using $Pr_{in}(m)$, the field enhancement in the ring, $Pr_{out}(m)/P_{in}$, is measured. The initial values for the iterative procedure are $P_{in}, \gamma(1) = \gamma_p, Er_{out}(1) = cE_{in}$ and $Er_{in}(1) = E_{in} * (-js)$, where γ_p is the passive loss in the ring.

$$\gamma(m) = \gamma_p e^{\frac{G_0 L}{1+\frac{\sum_{i=1}^{m-1} Pr_{out}(i)}{P_{in}}}} \tag{3.5}$$

$$Er_{out}(m) = Er_{in}(m-1) * \gamma(m) \tag{3.6}$$

$$Pr_{out}(m) = Pr_{in}(m-1) * \gamma^2(m) \tag{3.7}$$

$$E_{out}(m) = cE_{in}(m) + Er_{out}(m) * (-js) \tag{3.8}$$

$$Er_{in}(m+1) = Er_{out}(m) * (c) + (-js)E_{in}(m) \tag{3.9}$$

$$Pr_{in}(m+1) = Pr_{in}(m) * \gamma^2(m)c^2 + s^2P_{in}(m) \tag{3.10}$$

The cutoff for the number of iterations is chosen by minimizing the error between the final responses obtained using the iterative procedure and using Equation 3.1. The field enhancement at steady state can be calculated directly using a 2-port network visualization of the structure. This can be expressed as in Equation 3.11 [14].

$$\frac{Pr_{out}}{P_{in}} = \frac{(1-c^2)\gamma^2}{(1-c\gamma)^2} \tag{3.11}$$

Theoretically, it can be deduced from the sequence of Equations from 3.5 to 3.10 that γ at steady state decreases monotonically with increase in the ratio $\frac{P_{in}}{P_{sat}}$. However, the effective loss never falls below the passive value, meaning there is always a gain in the ring for any input.

CHAPTER IV

TOLERANCE ANALYSIS

The sensitivity of the response of an optical filter constructed with respect to the variations in an optical parameter is an important factor to decide the robustness. Major parameters that affect the response include coupling ratio, loss, wavelength and phase. A change in the response of an optical device can be measured using different factors. For a device like an optical filter, the response is primarily defined by the 3-dB Bandwidth, stopband rejection and passband gain. The amount of change in the response can be represented by the amount of change in the above parameters.

In [15], where a general design algorithm is presented for infinite impulse response bandpass filters, a study on the tolerance of parameters like coupling ratios and phases has been presented by using an analysis over 1000 runs of variations of a uniform distribution. Research on tolerance analysis of the optical parameters has been limited over the previous years. A detailed analysis of such a study for different optical parameters in a given optical circuit is presented in the following sections.

A. Algorithm

Two approaches are presented, one based on measuring the yield for a given tolerance and the other based on measuring the tolerance for a given yield. For a set of N input values to a parameter, the percentage of times the change in final response with respect to the ideal response is within a predefined value is known as the yield of the optical circuit with respect to that parameter.

1. Tolerance to Yield

An ideal response is defined as the magnitude response of the optical circuit when the values of all the parameters are exactly equal to the calculated values. The maximum amount of variation in the value of a parameter can be pre-defined based on the results of previous fabrications. A uniform random distribution is used to define a set of 1000 input values for the parameter. The range of the values is limited to within the maximum variation. For each input value from the set, the response of the optical circuit is calculated. The amount of variation in this response with respect to the ideal response is measured. A histogram of the variation over the 1000 input values is studied to find the tolerance of the circuit to that parameter.

2. Yield to Tolerance

The amount of yield required is predefined. For different values of maximum variation allowed in a parameter, a uniform distribution of 1000 input values is used to find the yield. The cutoff for the maximum variation allowed is obtained for the required yield.

B. Design

The above algorithm is implemented on a complex optical circuit that is designed to obtain a bandpass filter response of required specifications. Fig. 7 represents the fundamental block of the optical circuit under consideration, called the unit cell. On each of the upper and lower arms of the final design, a number of unit cells are used with slight changes in the values of their parameters. The unit cell is split into two parts for easier understanding, which can be noted in Fig. 7.

The feedback path consists of a microdisk coupled to a straight waveguide. This

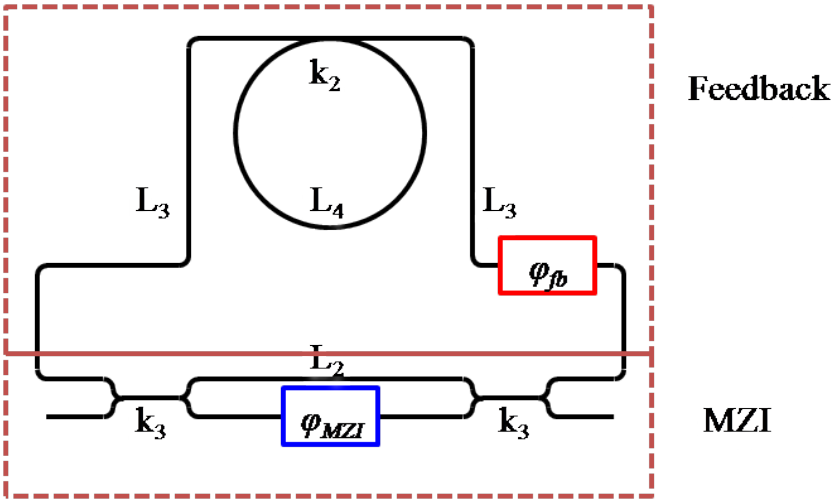

Fig. 7.: Unit cell

is in order to create a group delay corresponding to the required free spectral range for the design. A phase shifter is attached to the straight waveguide to control the resonant frequencies of the final response. The lengths in the feedback path are as follows. The straight waveguide length is $L_3 = 71.2080\mu m$, the perimeter of the microdisk is $L_4 = 125.6637\mu m$. The loss in the microdisk defined per unit length is $\alpha = 0.728dB/cm$. The group index of the substrate silicon is 4.135, while the effective index used for waveguide 2.356 and effective index for the microdisk is 2.7. The loss in the waveguide defined per unit length is $\alpha = 7dB/cm$. The coupling ratio between the disk and the waveguide is $k_2 = 0.06$. The feedback phase is one of the parameters used to optimize the final response.

The other part of the unit cell, an MZI, is shown in Fig. 7. The value of the coupling ratio used is $k_3 = 0.82$. A phase shifter each is included in each of the arms with the value of one as the negative of the other. The lengths of the waveguides are $L_2 = 170.6239\mu m$. The MZI phase shifter is the other parameter used for

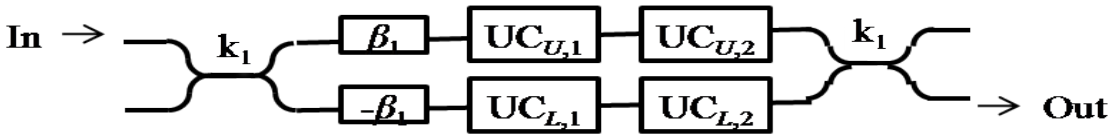

Fig. 8.: Baseline design

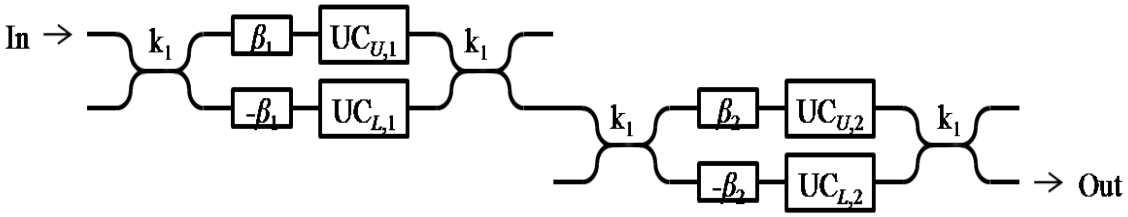

Fig. 9.: Cascade design

optimization of the final response. The unit cell is a single pole-single zero filter. The lengths and the coupling ratios in the unit cell are chosen such that a group delay of $100ps$, corresponding to an FSR of $10GHz$, is achieved.

Depending on the location and the number of unit cells in the circuit, bandpass responses of different 3dB Bandwidths and passband gains are obtained. Four designs are considered for the analysis. The first two are baseline lattice designs shown in Fig. 8, with the only difference between them being the passband gain. It is denoted by 4x1x1 implying there are 4 unit cells in each stage, 1 stage and repeated once. The latter two designs, called cascade designs, are shown in Fig. 9 with a difference in the value of passband gain. It is denoted by 2x1x2 implying there are 2 unit cells in each stage, 1 stage and repeated twice. The value of the coupler is set to $k_1 = 0.5$. A comparative study is done based on the number of unit cells used and their positions.

C. Setup

The tolerance analysis is done on the following parameters of the circuit - the coupling ratio of the microdisk in a unit cell, the coupling ratio of the MZI structure in a unit cell, the loss in the microdisk and the central wavelength over which the circuit is designed. For any parameter, variations in all unit cells of the design are random and are input simultaneously. The range of the maximum allowed variations in a parameter is chosen based on the parameter - from 1 to 10% in couplers, from 6 to 15% in losses and from 0.25 to 2.5pm in the central frequency.

The simulations are run for 10 different tolerance values for any parameter being varied. For each of the tolerances, a set of 1000 inputs is chosen. The total number of inputs, 10000 in this case, are maintained the same for all parameters and designs, with only a difference in scaling and translation. Also, an equal number of inputs is chosen between any two consecutive tolerance values.

CHAPTER V

NONLINEARITY ANALYSIS

Two types of Nonlinearities have been used for the analysis: Kerr nonlinearity and two photon absorption. The effects of these nonlinearities on an optical circuit are studied. The designs used for the analysis are the same ones as used for the tolerance analysis, baseline and cascade designs, to obtain a bandpass filter response of given specifications as discussed in Section B of Chapter IV. The nonlinearities have been discussed in detail in [16] and [17].

A. Nonlinearities

The Kerr Nonlinearity occurs due to the dependence of the refractive index on the intensity of the electric field applied. The change in the refractive index leads to a change in the phase of the waveguide [17]. Equation 5.1 shows the relation.

$$\frac{d\phi}{dL} = k_0 \Delta n P_{circ} \tag{5.1}$$

where the left side represents the change in phase per unit length, k_0 is the free space propagation constant, Δn is the change in refractive index, given by $\Delta n_{wvg} = 5.2 * 10^{-8}/mW$, $\Delta n_{disk} = 2.1 * 10^{-8}/mW$ and P_{circ} is the power circulating in the waveguide.

Two-photon absorption is the process in which two photons are absorbed simultaneously (a time difference of less than a nanosecond) by an electron, and the electron is excited to a state which has the energy equal to the sum of the energies of the photons. An intermediate stage is not necessary during this excitation. The amount of power absorbed is proportional to the square of the input power and hence

it is a nonlinear process [18]. Equation 5.2 represents this dependence.

$$\frac{dP}{dL} = -\alpha P_{circ}^2 \tag{5.2}$$

where α is the absorption coefficient per unit power per unit length, P_{circ} is the power circulating in the waveguide.The loss generated is given in Equation 5.3.

$$\gamma_{tpa} = e^{-\alpha P_{circ} L} \tag{5.3}$$

where L is the length of the waveguide, $\alpha_{wvg} = 7.4 * 10^{-4}/mW/cm$ and $\alpha_{disk} = 3 * 10^{-4}/mW/cm$.

B. Algorithm

In an optical circuit, the amount of power circulating in each waveguide is calculated in terms of the input power to the circuit. For a straight waveguide, P_{circ} is the square of the loss, γ, in the waveguide times the input power to it. For a coupler, the ratio is equal to the square of the coupling ratio. In case of a ring, the circulating power can be calculated by using the field enhancement shown in Equation 3.11.

For each of the nonlinearities under consideration, the extra loss generated is measured from equations 5.1 and 5.2. The response of the optical circuit is calculated with the incorporation of the new losses into the waveguide. The change in the response can be measured in terms of the passband gain, 3-dB bandwidth and stopband rejection. Since the effective loss depends on the input power to the circuit, the amount of variation in the final response is dependent on it as well. This can be used to find the cutoff input power at which the variation exceeds a predefined value.

CHAPTER VI

GAIN SIMULATIONS

A. Passive Structure

The iterative algorithm in Chapter III is implemented on a microring structure. The loss of the ring waveguide is set to $\gamma = 0.7943$. The group index of the substrate used is 3.63 and the effective index is 2.7. The radius of the microring is set to 2um. Simulations are run for a central wavelength of 1.55um. The coupling ratio between the ring waveguide and the straight waveguide is set to $k = 0.02$. The phase of the ring is set to zero.

The cutoff value for the number of iterations is obtained by minimizing the error. 100 iterations have been used which brought down the error to the order of 10^{-5}. The plot in Fig. 10 shows the decrease in error value for a P_{in}/P_{sat} value of 0.01. For $P_{in}/P_{sat} = 0.01$, the plot in Fig. 11 shows the comparison between the magnitude response obtained using the code and formula for the chosen cutoff value. Fig. 12 gives the comparison between the field enhancements obtained using the iterative algorithm and Equation 3.11 for different values of the passive loss. The value of the ratio P_{in}/P_{sat} used is 0.01. Increase in the number of iterations decreases the error between the two plots. A tradeoff is made between error and computation time. For any value of P_{in}, the transfer function E_{out}/E_{in} remains the same since the gamma value remained constant.

B. Microring with Gain

The amount of gain introduced into the ring at any time depends on the input signal power to the ring. The following results use Equation 3.4. The variation of

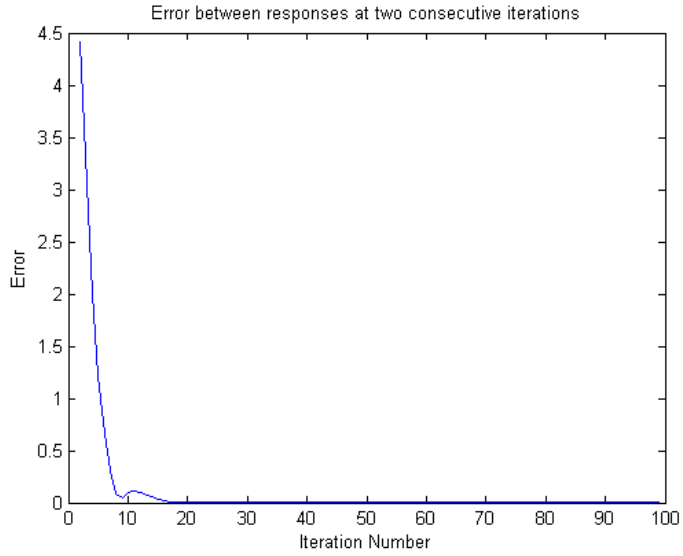

Fig. 10.: Error between magnitude response at two consecutive iterations

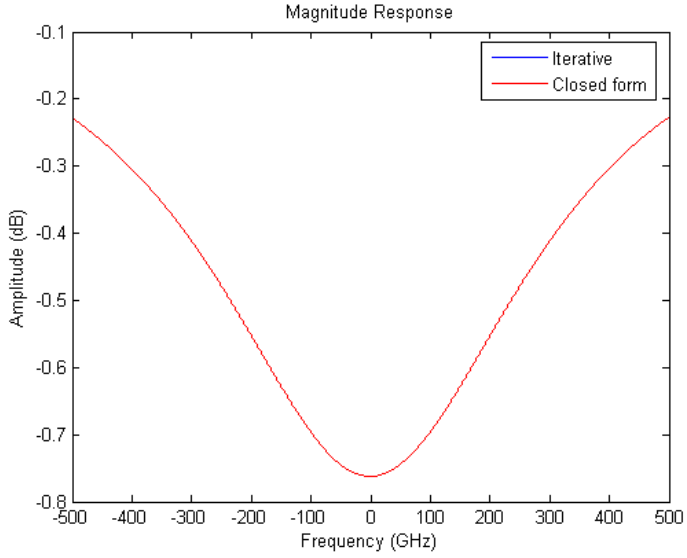

Fig. 11.: Magnitude response plots using iterative procedure and using closed form solution

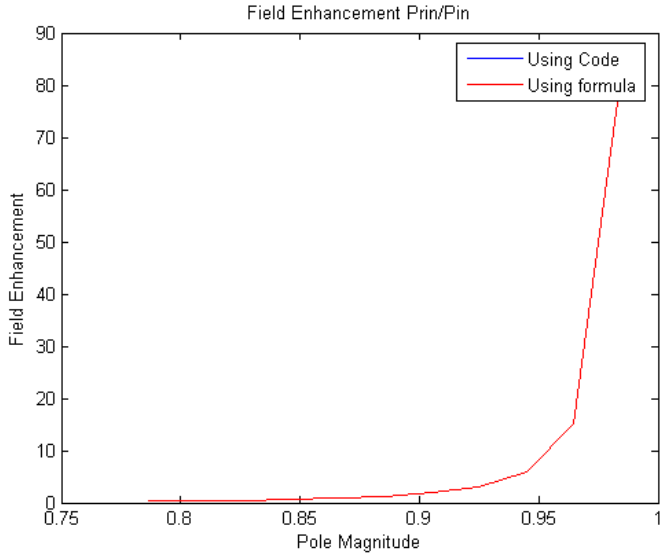

Fig. 12.: Field enhancement using iterative procedure and using closed form solution

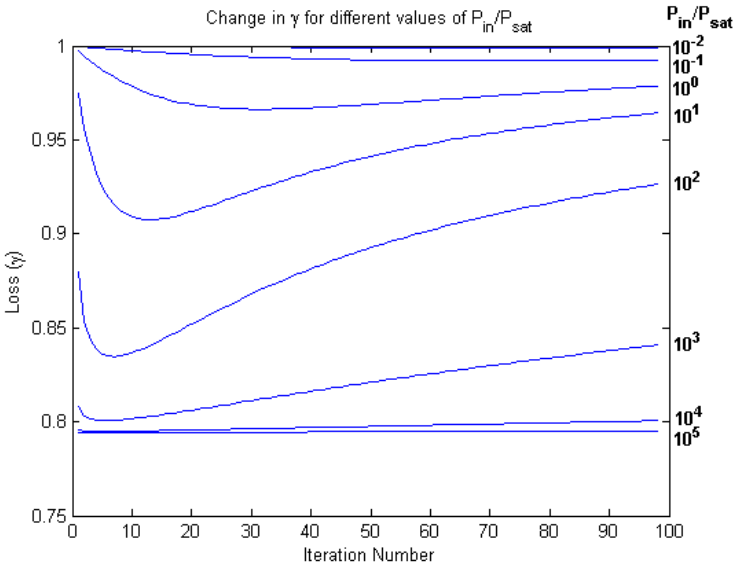

Fig. 13.: Change in γ for different values of $\frac{P_{in}}{P_{sat}}$

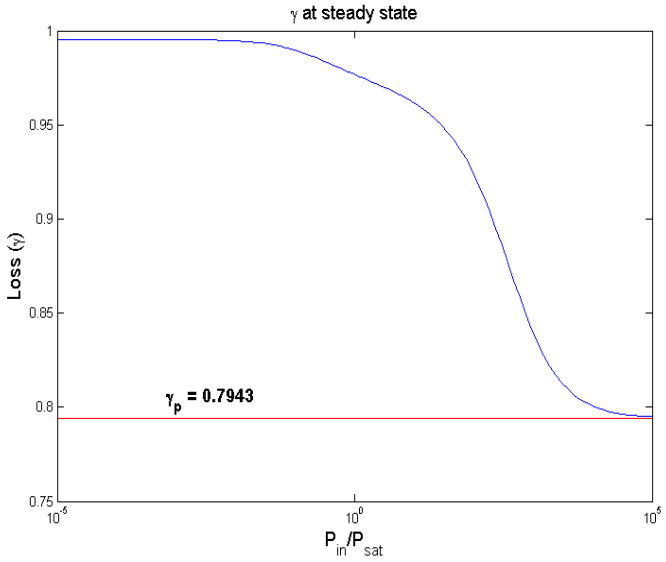

Fig. 14.: γ at steady state for different values of $\frac{P_{in}}{P_{sat}}$

gain as the ring reaches the steady state is plotted in the Fig. 13 for different values of P_{in}/P_{sat}. It gradually saturates to a value that is dependent on the input signal power, but is always greater than the passive loss γ_p. The saturated value of γ is plotted against the ratio P_{in}/P_{sat} in Fig. 14.

CHAPTER VII

TOLERANCE SIMULATIONS

A. Design Responses

The design used for the analysis is as described in Section B of Chapter IV. The specifications for the design are as follows - to obtain a bandpass response of 50MHz bandwidth over a free spectral range of 10GHz with a stopband rejection of 60dB. Using the parameter values as given in section B of Chapter IV, an optimization algorithm is run over the feedback phase and mzi phase of each unit cell. They are optimized to obtain the pole magnitude and phase of the required final design. The optimal values are given in the appendix.

The plot in Fig. 15 shows the magnitude, phase and group delay of a unit cell. It can be observed that the delay drops from $110ps$ at zero frequency to $30ps$ at $\pm 5GHz$. The change in group delay over the FSR of $10GHz$ effects the yield of central wavelength, as discussed later in the chapter. R_p is defined as the passband loss in the response in dB. The plots on Fig. 16 and Fig. 17 show the Magnitude responses for the baseline designs with -12dB and -18dB passband gains. The plots on Fig. 18 and Fig. 19 show the Magnitude responses for the cascade designs with -12dB and -18dB passband gains.

B. Tolerance Results

In both baseline and cascade designs, the 3-dB Bandwidth for the -12dB case is smaller than the other. Between baseline and cascade, the 3-dB Bandwidth is better in case of the former. The designs were optimized to get the specs of bandpass response as close to the required specs as possible. The 3dB bandwidths and stopband

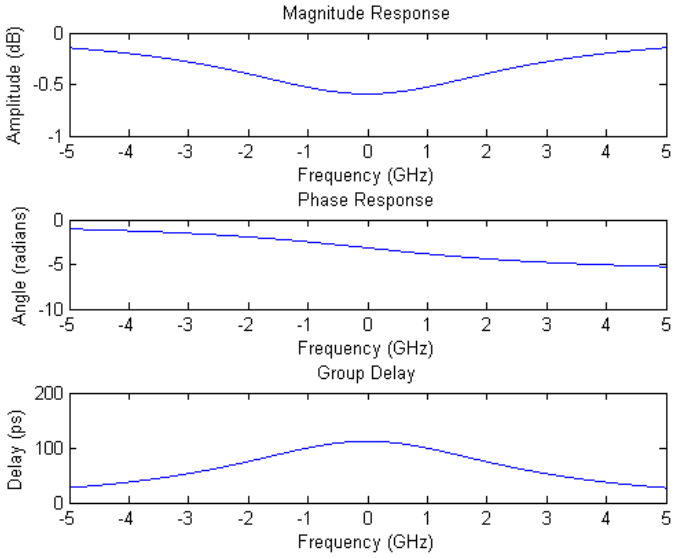

Fig. 15.: Magnitude, phase responses and group delay of a unit cell

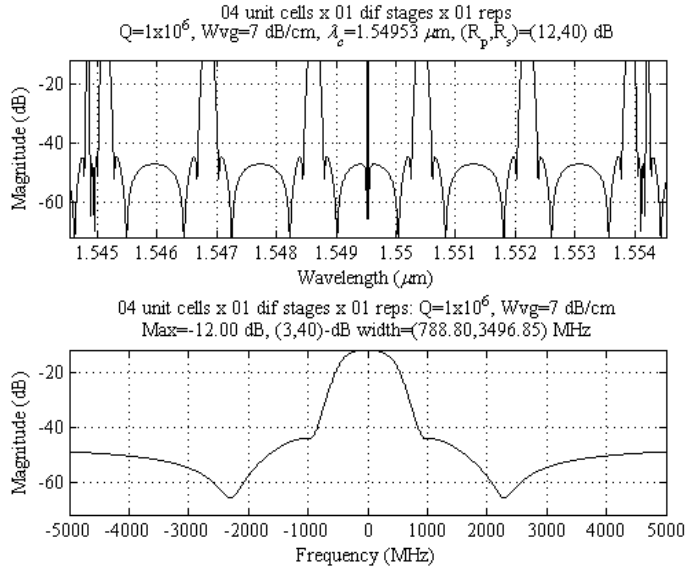

Fig. 16.: Magnitude response across (top) broadband and (bottom) narrowband for baseline design: $R_p = 12dB$

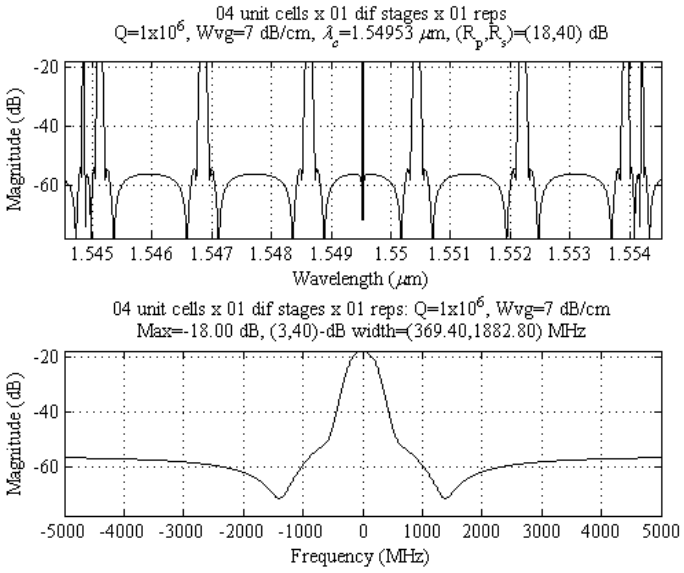

Fig. 17.: Magnitude response across (top) broadband and (bottom) narrowband for baseline design: $R_p = 18dB$

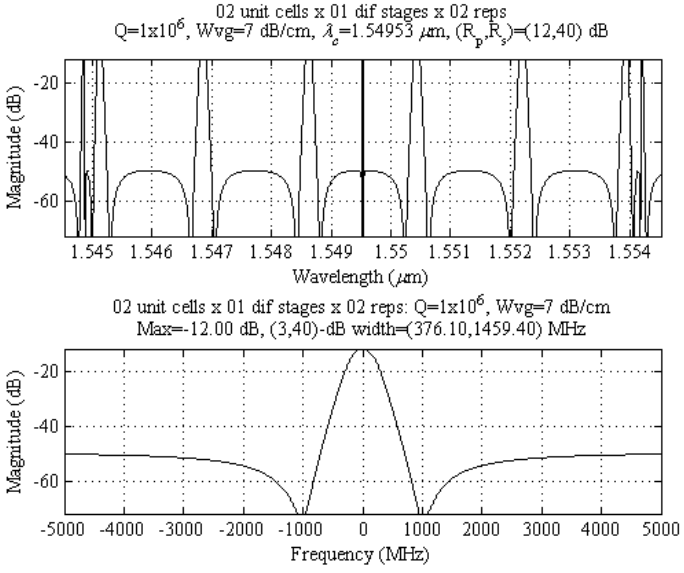

Fig. 18.: Magnitude response across (top) broadband and (bottom) narrowband for cascade design: $R_p = 12dB$

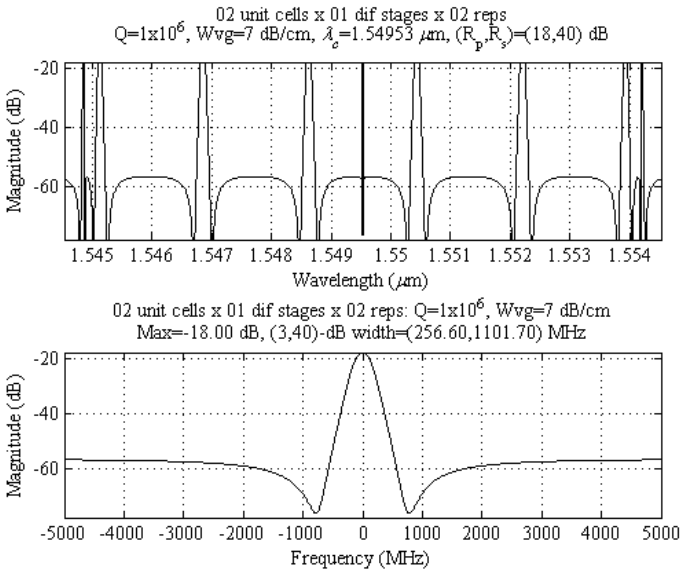

Fig. 19.: Magnitude response across (top) broadband and (bottom) narrowband for cascade design: $R_p = 18dB$

rejections for the responses obtained are noted in Figures 16 through 19.

k-disk:

The value of the microdisk coupler in each unit cell is $k = 0.06$. The range of the maximum allowed variation is from 1 to 10%. For each of these values, the final response is calculated and its parameters are measured.

The affect of a variation of 5% in the 3dB bandwidth, passband gain or stopband rejection on the response is minimal. The maximum variation allowed in the final response is hence limited to 5%. For each of the tolerance values, a set of 1000 inputs, varied from the original value in a uniform random distribution, is used. The number of times from the 1000 inputs where the variation in 3-dB bandwidth, passband gain and stopband rejection fall within this limit counts towards the yield for the parameter that is being varied. A plot of the curve, yield vs tolerance, is shown in Fig. 20 for

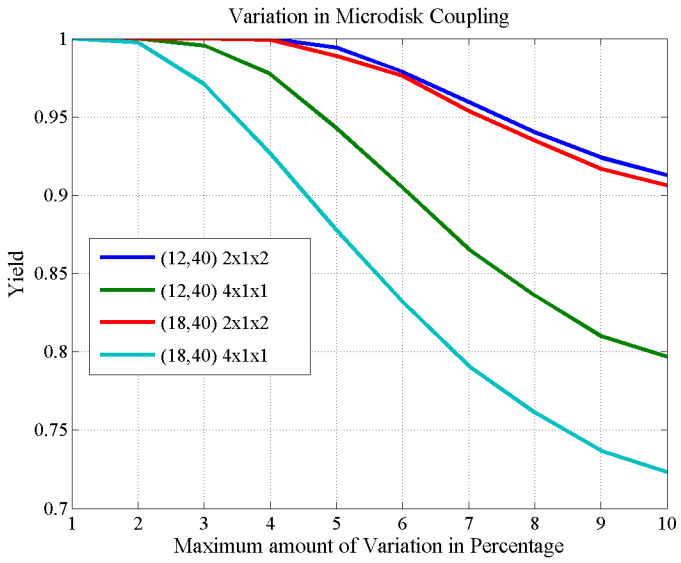

Fig. 20.: Yield for microdisk coupler

each of the four designs.

k-mzi:

The value of the mzi coupler in each unit cell is $k = 0.82$. The range of the maximum allowed variation is from 1 to 10%. In any unit cell, the variation in both of the couplers is always kept the same. The analysis is done as in the case of the k-disk. The histogram of the 3-dB Bandwidth, passband gain and stopband rejection for the baseline: -12 dB passband gain case are shown in Figures 21 through 23 for a tolerance value of 5%. The worst case response based on the worst case 3-dB Bandwidth is shown in Fig. 24. The yield plot is shown in Fig. 25.

Q-disk:

The value of the quality factor of the mircodisk in each unit cell is $Q = 10^6$. The range of the maximum allowed variation is from 6 to 15%. The yield plot is shown in Fig. 26.

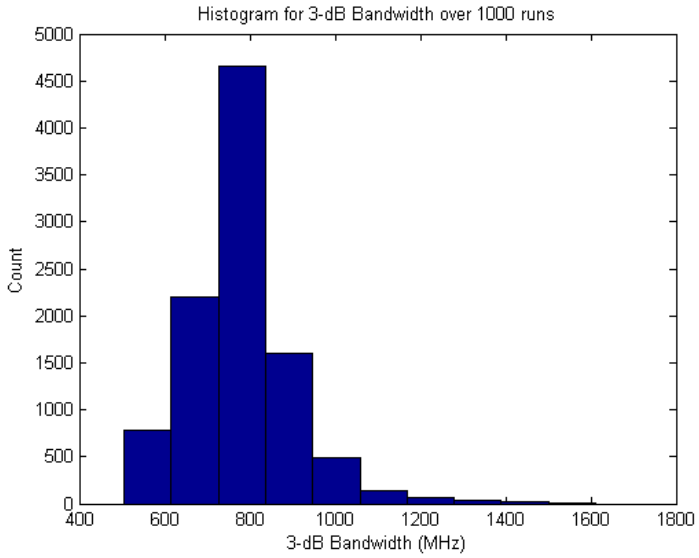

Fig. 21.: Histogram for 3dB bandwidth for variation in MZI coupler of baseline $R_p = 12dB$ design

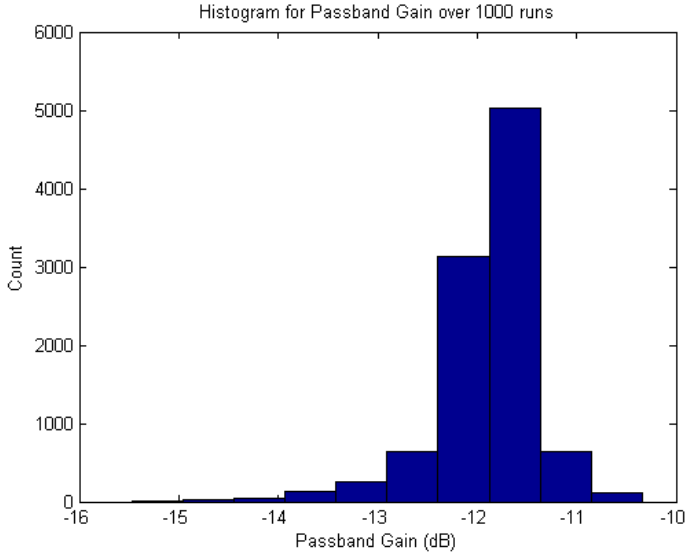

Fig. 22.: Histogram for passband gain for variation in MZI coupler of baseline $R_p = 12dB$ design

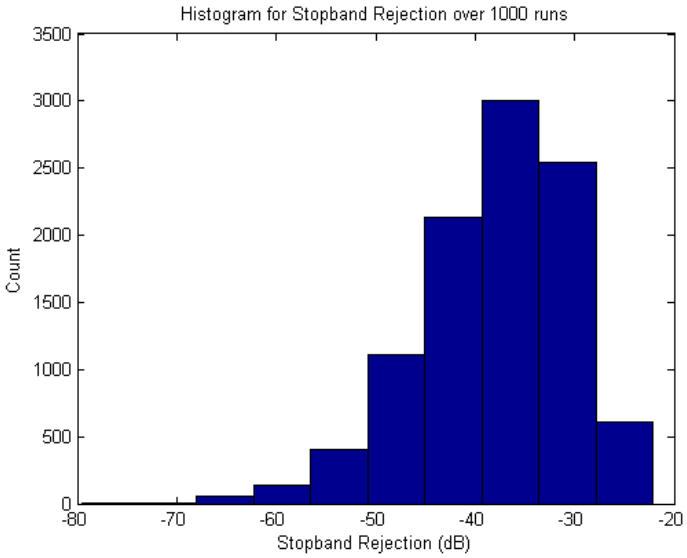

Fig. 23.: Histogram for stopband rejection for variation in MZI coupler of baseline $R_p = 12dB$ design

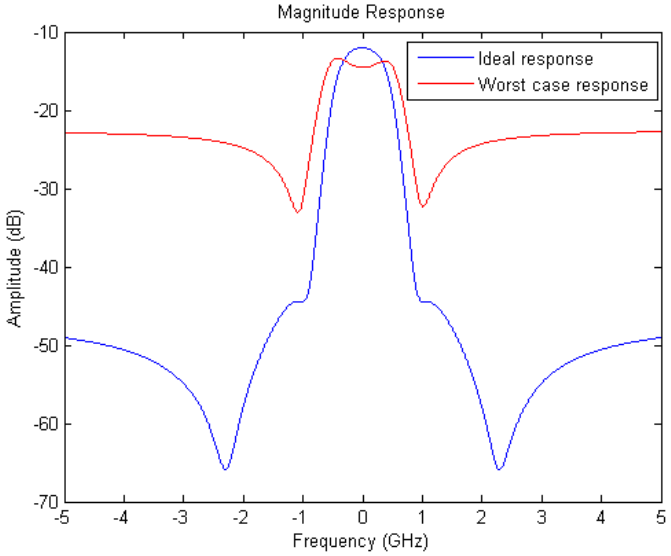

Fig. 24.: Magnitude response for worstcase 3dB bandwidth for variation in MZI coupler of baseline $R_p = 12dB$ design

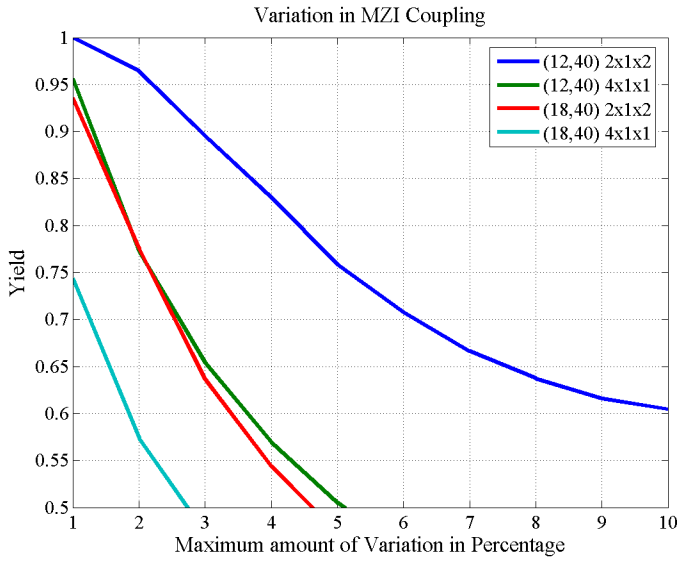

Fig. 25.: Yield for MZI coupler

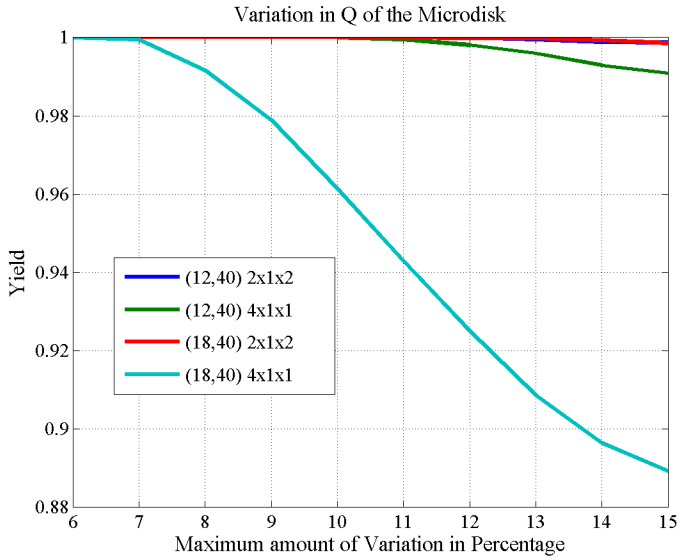

Fig. 26.: Yield for loss in microdisk

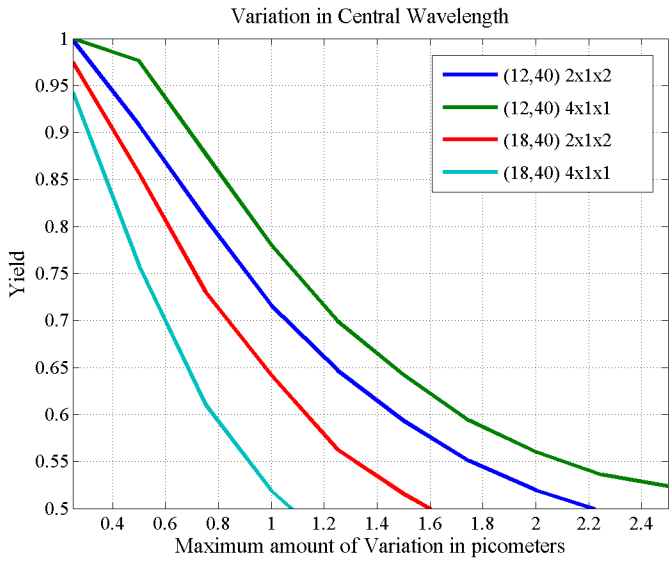

Fig. 27.: Yield for central wavelength

Central Wavelength:

The value of the central wavelength over which the circuit is designed is $\lambda_0 = 1.55\mu m$. An equal variation in the central wavelength of all unit cells causes the final response to shift. Because of different amounts of variations in each unit cell, the final response gets distorted for higher tolerance values. Hence, the range of the maximum allowed variation is limited to the range 0.25 to 2.5 μm on central wavelength. The tolerance analysis is repeated and the yield plot is shown in Fig. 27. The amount of yield drops drastically even for variations in the order of picometers. This is because of the variation in group delay over the FSR of the design as shown in Fig. 15. As the central wavelength is varied by different amounts in different unit cells, the shifts that occur in the response as a result are also different, which leads to a high distortion in the final response. This can be minimized by obtaining a constant group delay for the unit cell, over the FSR.

Table I.: Range of variations in 3dB bandwidth, passband Gain and stopband rejection over 1000 simulations

Design	3-dB Bandwidth	Passband Gain	Stopband Rejection
Baseline $R_P = 12dB$	500:1600	-15.5:-10.5	-80:-22
Baseline $R_P = 18dB$	100:900	-25:-14	-90:-25
Cascade $R_P = 12dB$	320:630	-24:-11	-100:-35
Cascade $R_P = 18dB$	100:440	-37:-12	-115:-40

The range of variation in 3-dB bandwidth, stopband rejection and passband gain for variation in k-mzi are tabulated in Table I for each of the four designs.

C. Inferences

- For a given design and given parameter for variation, the yield decreases with the increase in tolerance value of the parameter.
- For a given tolerance of a parameter and given passband gain, the baseline structure has a lesser yield than cascade. One exception is in the case of variation in the central wavelength.
- For a given tolerance of a parameter and given type of design, the yield is always greater for lower magnitude of passband gain.
- For an expected yield of 95%, the maximum allowed variations are 7.35% for microdisk coupling ratio, 2.2% for MZI coupling ratio, $> 10\%$ for Quality factor of the microdisk and 0.38 pm for the central wavelength.
- Increasing the maximum allowed variation in the final response increases the yield and hence increases the tolerance for all the parameters.

CHAPTER VIII

NONLINEARITY SIMULATIONS

A. Results

The designs used for the nonlinearity analysis are the same as the ones used for the tolerance analysis. The analysis has been run for the input power range of 1mW to 5mW. The losses generated because of the nonlinearity are simulated. They are introduced into the design, apart from the original losses in the waveguide. The changes in the final responses from the original response are measured in terms of 3dB bandwidth and passband gain.

Fig. 28 shows the magnitude response with nonlinearity included for different levels of input power for the baseline structure with -12dB passband gain. Fig. 29 shows the same for the cascade structure with -12dB Passband Gain.

Tables II and III respectively show the additional losses and phases in the baseline $R_p = 12dB$ design due to two photon absorption and kerr nonlinearity. Table IV shows the maximum transmission in a disk of the unit cell for calculating the input power at subsequent disks for the baseline $R_p = 12dB$ and cascade $R_p = 12dB$ designs.

B. Inferences

- Increase in input power lowers the passband gain.
- Input power effect on 3-dB bandwidth depends on structure. It decreases with increase in the power level for the Baseline structure and viceversa for the Cascade structure.
- The non-linearity effect is smaller for more number of stages (division of power).

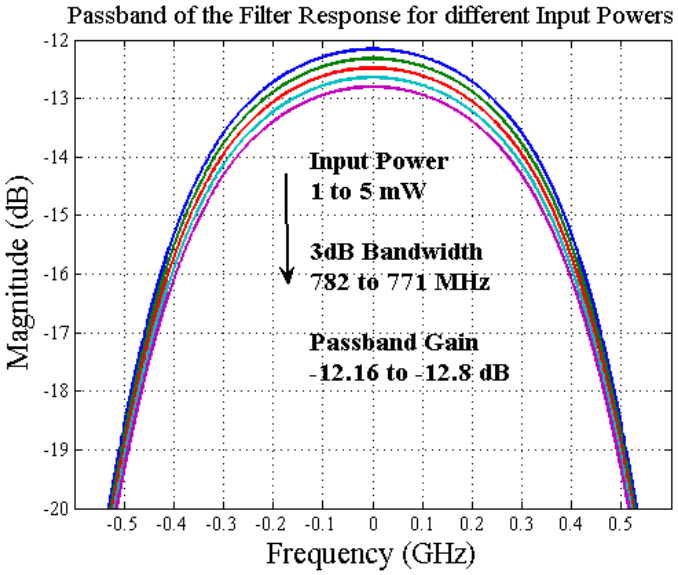

Fig. 28.: Magnitude response with nonlinearity: baseline $R_p = 12dB$ design

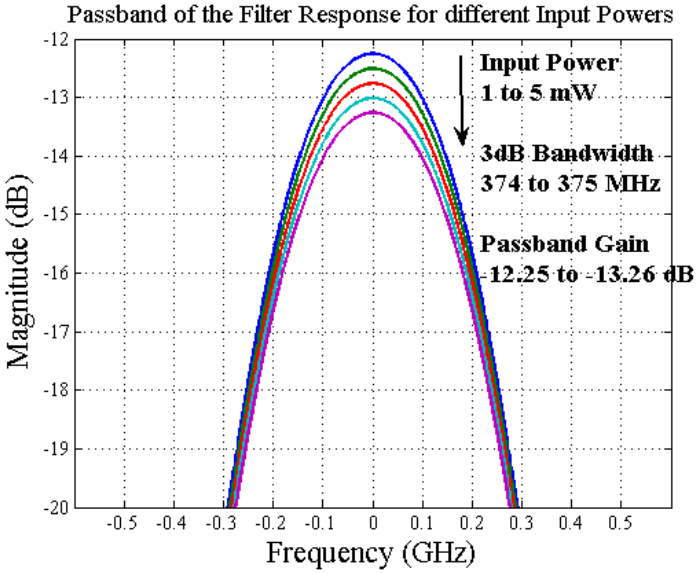

Fig. 29.: Magnitude response with nonlinearity: cascade $R_p = 12dB$ design

Table II.: Additional loss in the disks in the unit cells for different input powers (refer Fig. 8 for the abbreviations in the first row)

Input power (mW)	$UC_{U,1}$	$UC_{L,1}$	$UC_{U,2}$	$UC_{L,2}$
1	0.999953	0.999953	0.999988	0.999988
2	0.999906	0.999906	0.999976	0.999976
3	0.999859	0.999859	0.999964	0.999964
4	0.999812	0.999812	0.999953	0.999953
5	0.999766	0.999766	0.999941	0.999941

Table III.: Additional phase in the disks in the unit cells for different input powers (refer Fig.8 for the abbreviations in the first row)

Input power (mW)	$UC_{U,1}$	$UC_{L,1}$	$UC_{U,2}$	$UC_{L,2}$
1	$-0.0398 * 10^{-6}$	$-0.0398 * 10^{-6}$	$-0.0100 * 10^{-6}$	$-0.0100 * 10^{-6}$
2	$-0.0796 * 10^{-6}$	$-0.0796 * 10^{-6}$	$-0.0200 * 10^{-6}$	$-0.0200 * 10^{-6}$
3	$-0.1195 * 10^{-6}$	$-0.1195 * 10^{-6}$	$-0.0299 * 10^{-6}$	$-0.0299 * 10^{-6}$
4	$-0.1593 * 10^{-6}$	$-0.1593 * 10^{-6}$	$-0.0399 * 10^{-6}$	$-0.0399 * 10^{-6}$
5	$-0.1991 * 10^{-6}$	$-0.1991 * 10^{-6}$	$-0.0499 * 10^{-6}$	$-0.0499 * 10^{-6}$

Table IV.: Maximum transmission in the disks in the unit cells for different designs (refer Fig. 8 for the abbreviations in the first row)

Design	$UC_{U,1}$	$UC_{L,1}$	$UC_{U,2}$	$UC_{L,2}$
Baseline $R_p = 12dB$	-4.4722	-4.4722	-5.4589	-5.4589
Cascade $R_p = 12dB$	-4.9658	-4.9658	-4.9658	-4.9658

CHAPTER IX

CONCLUSION

It has been shown that the response of a ring with gain can be obtained using time domain simulation. The algorithm has been proven against the steady state frequency response in the case of passive structures. The gain dependence on power input to the ring - average power over a continuous signal and instantaneous power for an impulse - have been considered and compared.

The designs to obtain the bandpass response with given specifications are studied. The difference in the location and number of unit cells on an arm in the design changes the 3dB bandwidth of the final response. The tolerance analysis of these designs is presented. It has been shown that the use of 1000 different sets of inputs is sufficient as the variance of the sets matches the variance of the range of the values. Use of the same set of uniform variations for different designs helped during their tolerance comparison.

The tolerance of the loss in a waveguide has been found to be much higher than that for couplers and central wavelength of the microdisk used for the variable delay line. Between the couplers, the disk coupler in the unit cell has a higher tolerance than that of the mzi coupler in case of all four designs investigated. Even a tiny amount of change in the central wavelength has effected the final response by a large percentage. A constant group delay over the free spectral range increases the yield with respect to central wavelength.

The Kerr nonlinearity and the two-photon absorption have both been introduced into the designs used for tolerance analysis. The amount of change in phase because of Kerr nonlinearity has been found to be smaller than the effect of two photon absorption on the extra loss. The dip in the passband gain for different power levels

is because of the two-photon absorption.

The algorithm used for the gain analysis has been used only in case of microring. It can be tested on more complex designs and analyzed. The exact dependence of the gain on the input power can be established by looking into a larger number of designs, in a simulation point of view. The nonlinearity simulations have considered two of the major nonlinearities. Introduction of more of them can distort the response further, which can be explored.

REFERENCES

[1] B. Moleshi, J.W. Goodman, M.Tur, H.J. Shaw. Fiber-optic lattice signal processing. In *Proc. of IEEE*, volume 72, no. 7, pages 909-930, July 1964.

[2] J. Campany and M.A. Muriel. A new transfer matrix formalism for the analysis of fiber ring resonators: compound coupled structures for FDMA demultiplexing. *Journal of Lightwave Technology*, 8(12):1904-1919, 1990.

[3] E.C. Heyde and R.A. Minasian. A solution to the synthesis problem of recirculating optical delay line filters, *IEEE Photonics Technology Letters*, 6(7):833-835, 1994.

[4] N.Q. Ngo and L. Nyugen Binh. Novel realization of monotonic butterworthtype lowpass, highpass, and bandpass optical filters using phase-modulated fiber-optic interferometers and ring resonators. *Journal of Lightwave Technology*, 12(5):827-841, 1994.

[5] C.K. Madsen. Optical all-pass filters for phase response design with applications for dispersion compensation. *Journal of Lightwave Technology*, 10(7):994-996, 1998.

[6] C.K. Madsen. Efficient architectures for exactly realizing optical filters with optimum bandpass designs. *Journal of Lightwave Technology*, 10(8):1136-1138, 1998.

[7] C.K. Madsen and J.H. Zhao. Optical Filter Design and Analysis: A Signal Processing Approach. John Wiley and Sons, Ltd, Newyork, NY, 1999.

[8] P.G. Kik and A. Polman. Erbium doped optical waveguide amplifiers on silicon. *MRS Bulletin*, 23(4):48-54, 1998.

[9] A. D'Orazio, M.D. Sario, L. Mescia, V. Petruzzelli and F. Prudenzano. Optical amplification for communication systems. In *Proc. of International Conference on Transparent Optical Networks*, volume 1, pages 119-125, Warsaw, Poland, 1964.

[10] P. Urquhart and O.G. Lopez. Optical amplifiers for telecommunications. In *Intelligent Signal Processing IEEE International Symposium*, 23(4):1-6, 2007.

[11] J. Jahn and K.H. Brennerl. Optical amplifiers for telecommunications. *Microoptics: From Technology to Applications*, Springer-Verlag, New York, 2004.

[12] K. Takada, M. Oguma, H. Yamada, S. Mitach and M. Golling. Gain distribution measurement of an erbium-doped silica-based waveguide amplifier using a complex OLCR. *IEEE Photonics Technology Letters*, 9(8):1102-1103, 1997.

[13] R. Salas-Montiel, M.E. Solmaz, O. Eknoyan and C.K. Madsen. Er-doped optical waveguide amplifiers in x-Cut lithium niobate by selective codiffusion. *IEEE Photonics Technology Letters*, 22(6):362-364, 2010.

[14] J.E. Heebner and R.W. Boyd. Enhanced all-optical switching by use of a nonlinear fiber ring resonator. *Optics Letters*, 24(12):847-849, 1999.

[15] C.K. Madsen. General IIR optical filter design for WDM applications using allpass filters. *Journal of Lightwave Technology*, 18(6):860-868, 2000.

[16] M.N. Islam. *Ultrafast Fiber Switching Devices*, Cambridge University Press, New York, 1992.

[17] R.W. Eason and A. Miller. *Nonlinear Optics in Signal Processing*, Chapman and Hall, London, UK, 1993.

[18] W. Kaiser and C.G.B. Garrett. Two-photon excitation in CaF2:Eu2+. *Physics Rev. Letters*, 7(6):229:231, 1961.

APPENDIX A

DESIGN VALUES

Tables V through VIII give the values of the feedback, mzi and β phases of all the unit cells that are used to optimize the final response of the designs used for tolerance and nonlinearity analyses.

Table V.: Optimal values of the phases in baseline $R_p = 12dB$ design

Baseline $R_P = 12dB$	ϕ_{mzi}	ϕ_{fb}	β
Upper arm unit cells	1.2158, 2.1179	0.6822, 0.3517	1.9743
Lower arm unit cells	-1.2158, -2.1179	-2.3879, -2.0574	-1.9743

Table VI.: Optimal values of the phases in baseline $R_p = 18dB$ design

Baseline $R_P = 18dB$	ϕ_{mzi}	ϕ_{fb}	β
Upper arm unit cells	2.4707, 1.9570	-0.1183, 0.0681	1.8767
Lower arm unit cells	-2.4707, -1.9570	-1.5874, -1.7738	-1.8767

Table VII.: Optimal values of the phases in cascade $R_p = 12dB$ design

Cascade $R_P = 12dB$	$\phi_m zi$	$\phi_f b$	β
Upper arm unit cells	1.9055, 1.9055	0.0520, 0.0520	1.8287, 1.8287
Lower arm unit cells	-1.9055, -1.9055	-1.7576, -1.7576	-1.8287, -1.8287

Table VIII.: Optimal values of the phases in cascade $R_p = 18dB$ design

Cascade $R_P = 18dB$	ϕ_{mzi}	ϕ_{fb}	β
Upper arm unit cells	2.1914, 2.1914	0.0305, 0.0305	1.6851, 1.6851
Lower arm unit cells	-2.1914, -2.1914	-1.7362, -1.7362	-1.6851, -1.6851

VITA

Name: Vivek Vandrasi

Address: Electrical Engineering Department
3128 TAMU
College Station, TX 77843-3128

Email: vivekvandrasi@neo.tamu.edu

Education: B.Tech in Electronics and Communication Engineering, 2008
Indian Institute of Technology (IIT) Guwahati
M.S. in Electrical Engineering, 2010
Texas A&M University

The typist for this thesis was Vivek Vandrasi.